

Quality Assurance in PET: Evaluation of the Clinical Relevance of Detector Defects

Ralph Buchert, Karl H. Bohuslavizki, Janos Mester and Malte Clausen

Department of Nuclear Medicine, University Hospital Eppendorf, Hamburg, Germany

Defective detector blocks in PET may cause serious image artifacts. To estimate the influence of malfunctioning detectors on image quality, a method is described for transferring the actual detector defect onto previously acquired scans. **Methods:** Consequences of detector defects of varying types and extensions were simulated in phantom studies as well as in clinical ^{18}F -fluorodeoxyglucose investigations. First, a condition frame was obtained by dividing the sinogram of a blank measurement, obtained with rod sources on the defective PET camera, by the sinogram of a reference blank acquired before the appearance of the defect. Second, the sinogram of a previously acquired typical patient study was multiplied by the condition frame and reconstructed. Thereafter, images from corrupted sinograms were compared visually with their originals. For repairing defective sinograms, linear interpolation and the constrained Fourier space method were tested. **Results:** The effects of detector defects can be simulated accurately in patient studies. The correction methods applied are especially helpful in cases of (a) several neighboring defective detectors and small study objects, (b) small hot artifacts and (c) several nonadjacent defective detectors. Linear interpolation is faster than the constrained Fourier space method; it is more widely applicable and provides similar results. **Conclusion:** The proposed approach allows specific evaluation of clinical consequences of detector defects. This technique simplifies the decision as to whether a planned patient study can be performed or must be postponed. Even in cases of serious detector problems, sinogram repair may help eliminate image artifacts and minimize the loss of image quality.

Key Words: PET; detector defect; sinogram; linear interpolation; constrained Fourier space method

J Nucl Med 1999; 40:1657-1665

An occasional problem in PET is a defect in one or more detector blocks of the scanner. Therefore, quality assurance is performed daily to document constancy of the scanner. However, quality assurance procedures usually do not support evaluation of the clinical relevance of recognized detector defects.

In the most widely used PET scanners made by CTI/Siemens, Inc. (Knoxville, TN), constancy checks are performed by comparing a reference blank scan obtained during

the last setup with a daily acquired conditional blank scan using rotating rod sources. The difference between the two scans is characterized by the value of the so-called average variance. This parameter is a sensitive indicator of all types of detector problems. When its value is elevated, sinograms of the actual blank scan should be checked carefully.

Detector problems should be considered from two viewpoints. Calling the manufacturer's service contact is recommended strongly even in cases of minor defects. However, these defects are not necessarily of clinical relevance. Moreover, several practical problems arise in postponing patient scans. Consequently, it is desirable to estimate accurately the effect of a specific problem on the clinical readability of PET images.

A method is described here that simulates the actual detector defect in previously acquired scans of the type considered for the next patient, e.g., brain scans. Visual comparison of the artificially distorted and original images enables the physician to decide whether the intended study can be performed without significant loss of readability. Moreover, the clinical usefulness of two different methods of sinogram repair was tested.

MATERIALS AND METHODS

Notation

The object to be reconstructed is denoted by $f(x,y)$. A second pair of Cartesian coordinates (s,t) is used to specify the projection geometry, in which (s,t) is rotated by the angle θ from (x,y) . The pair of parameters (s,θ) defines a line of integration (line of response) parallel to the t -axis and located at a (signed) distance s from the origin. Projection data are denoted by the usual sinogram representation $p(s,\theta)$. For quantification of changes in the difference between two sinograms or between two images, the usual root mean square measure denoted by d is used, i.e.:

$$d(p,p_0) = \sqrt{\sum_{s,\theta} [p(s,\theta) - p_0(s,\theta)]^2}, \quad \text{Eq. 1}$$

and

$$d(f,f_0) = \sqrt{\sum_{x,y} [f(x,y) - f_0(x,y)]^2}. \quad \text{Eq. 2}$$

Data Acquisition

Data were acquired on an ECAT EXACT 47 (921) scanner (CTI/Siemens) in standard two-dimensional mode (1). Blank scans

Received Jul. 13, 1998; revision accepted Mar. 26, 1999.

For correspondence or reprints contact: Ralph Buchert, PhD, Department of Nuclear Medicine, University Hospital Eppendorf, Martinistr. 52, D-20246 Hamburg, Germany.

were acquired using rotating ^{68}Ge -rod sources. Patient studies were performed using ^{18}F -fluorodeoxyglucose according to generally accepted standard protocols for heart, brain and whole-body investigations (2).

Defect Simulation in Blank Scans

To simulate detector defects, blank scans of rotating rod sources were used. Sinograms of the blank acquisition during the last setup of the scanner served as references. Blank scans with defective detectors were obtained either by turning off individual detectors or by simple mathematic modeling on the reference sinogram. In the latter case, values of individual elements $p(s,\theta)$ of the sinogram corresponding to the geometric position of the defective detectors were modified. Total loss of sensitivity was expressed by setting element values of the reference sinogram to zero; twofold-increased detector sensitivity was established by multiplying element values by two. The following detector defects were simulated: (a) zero sensitivity of one to four detector blocks (one bucket), (b) six equidistant detector regions each of 5° width with zero sensitivity and (c) twofold-increased sensitivity of half the crystals within one block and zero sensitivity of the remaining crystals in the block. One block affects 4% of the lines of response in the corresponding planes. The case of six equidistant detector regions with zero sensitivity mimics the detector gaps connected with the special geometric situation of six large crystals in a hexagonal configuration (i.e., PENN-PET [3]; UGM Medical Systems, Philadelphia, PA; QUEST family; GE Medical Systems, Waukesha, WI; or CPET; ADAC Laboratories, Milpitas, CA). The number of lines of response lost because of these gaps is the same as in the case of four defective blocks. The only sensitivity increases actually seen in real conditions are those of individual crystals within a block, when hits from other areas of the block are

assigned incorrectly. Therefore, simulation of increased sensitivity was restricted to half the crystals of a block, with zero sensitivity of the remaining crystals of the block.

Before additional handling, both reference and defective sinograms were smoothed by a $9 \times 9 \times 9$ smoothing using the kernel (4):

$$K_9(i,j,k) = K_9(i) \times K_9(j) \times K_9(k). \quad \text{Eq. 3}$$

$K_9(i) =$

$$(0.017 \ 0.102 \ 0.362 \ 0.776 \ 1 \ 0.776 \ 0.362 \ 0.102 \ 0.017). \quad \text{Eq. 4}$$

In addition, sinograms were normalized for source activity and acquisition time.

Defect Copy

A condition frame c was obtained by dividing the defective blank sinograms b element by element by the reference blank sinograms b_0 :

$$c(s,\theta) = b(s,\theta)/b_0(s,\theta). \quad \text{Eq. 5}$$

In this condition frame, elements not affected by the defect have a value close to 1, elements corresponding to cold detectors have a value of 0 and elements corresponding to lines of response with a twofold sensitivity have a value of 2 (Fig. 1, top row). Imaging features of the defective scanner were transferred to clinical studies by multiplying the sinograms p_0 of reference patient studies acquired earlier by the condition frame, i.e., corrupted sinograms p were simulated by:

$$p(s,\theta) = c(s,\theta) \times p_0(s,\theta) \quad \text{Eq. 6}$$

(Fig. 1, bottom row).

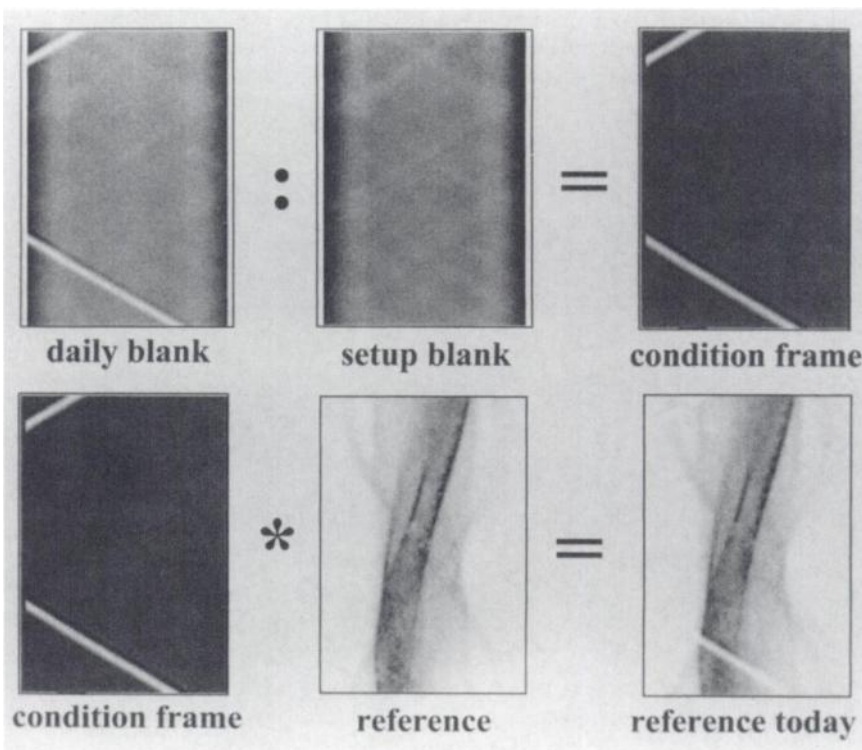


FIGURE 1. Defect copy: Condition frame parameterizing status of scanner is obtained by dividing raw data of scan with defect (daily blank) by raw data of scan of same source acquired before appearance of defect (setup blank). Defect is transferred to typical patient scan (reference) by multiplication with condition frame. Bright diagonal band with zero counts accompanied by smaller dark diagonal band of increased counts in sinogram of daily blank points to defective photomultiplier.

Sinogram Repair

To determine which elements of the sinograms of a patient study were to be repaired, a defect mask m was generated by determining thresholds for the condition frame. An element was marked as erroneous if its value in the condition frame was <0.9 or >1.1 , i.e.:

$$m(s,\theta) = \begin{cases} 1, & \text{if } |c(s,\theta) - 1| > 0.1 \\ 0, & \text{otherwise.} \end{cases} \quad \text{Eq. 7}$$

The values of the respective elements in the sinograms of the patient study were then estimated mathematically by the correction method applied. All other elements were assumed to be correct and, thus, remained unchanged. Two different methods of sinogram repair were investigated: linear interpolation and the constrained Fourier space method.

Sinogram Repair by Linear Interpolation

Elements marked as erroneous in the defect mask were calculated by one-dimensional linear interpolation within columns (view angle, θ direction) from the values of the adjacent noncorrupted elements. Before linear interpolation, statistical variation at these elements was reduced by 3×3 smoothing using the kernel:

$$K_3(i,j) = K_3(i) \times K_3(j), \quad \text{Eq. 8}$$

$$K_3(i) = (0.5 \quad 1 \quad 0.5). \quad \text{Eq. 9}$$

Elements not marked as erroneous in the defect mask were used during smoothing only. After interpolation a second 3×3 smoothing using the same kernel K_3 was applied at the repaired elements. The periodicity of the sinograms (Moebius band structure, $0 \leq \text{view angle} < \pi$) was considered at the upper and lower edge.

Sinogram Repair by Constrained Fourier Space Method

Two-dimensional Fourier transformation of a sinogram provides a matrix in which counts from sources within and outside the transaxial field of view of the scanner can be differentiated (5). In this context, a detector with total loss of sensitivity is a source lying outside the field of view and producing negative counts.

The constrained Fourier space method described by Karp et al. (6) is based on this property of the two-dimensional Fourier transformation of sinograms. On the Fourier-transformed sino-

gram, a vertical conic section represents the area to which counts originating outside the field of view contribute. Counts originating within the field of view are displayed within the remaining part of the matrix (Fig. 2). Hence, if elements in the vertical conic section are set to zero and an inverse Fourier transformation of the remaining Fourier coefficients is performed, an estimate of the affected parts of the corrupted sinogram can be obtained without distortion due to counts originating from the defective blocks. Because the separation of counts originating from the patient or from the defective detector is not complete in Fourier space, estimates are improved by iterating forward and inverse transformation several times. In phantom studies, 500 iterations were applied, whereas in patient studies iteration was stopped after the optimal number of iterations, i.e., when the root mean square distance d of the repaired sinogram from the reference sinogram reached a minimum.

To decrease computation time, sinograms were cut vertically to the object radius. Repair was restricted to those lines of response in the defect mask that crossed the study object. In our simulations, this was achieved from the knowledge of the uncorrupted sinograms. In real applications, the contour of the study object can be estimated from the uncorrupted parts of the sinograms.

Phantom Studies

To test the implementation of the constrained Fourier space method, a software phantom similar to the one described by Fujieda et al. (7) was considered. The phantom was a homogeneous disk of 20-cm radius at the center of the field of view, with one hot and two cold circular lesions of 5-cm radius (radius of transaxial field of view 28 cm) (Fig. 3). The cold lesions represented zero uptake, and the contrast of the hot lesion to the disk was 2.0.

Clinical Evaluation

For distortion of a reference patient study acquired by a properly operating scanner, a worst-case position of the defective detector blocks was established. In whole-body oncology studies, the blocks closest to a peripheral lymph node metastasis with a relatively low intensity were corrupted. After reconstruction, corrupted and reference images were compared visually.

For testing of sinogram repair, sinograms were corrupted using the condition frame as described above. Both sinogram repair

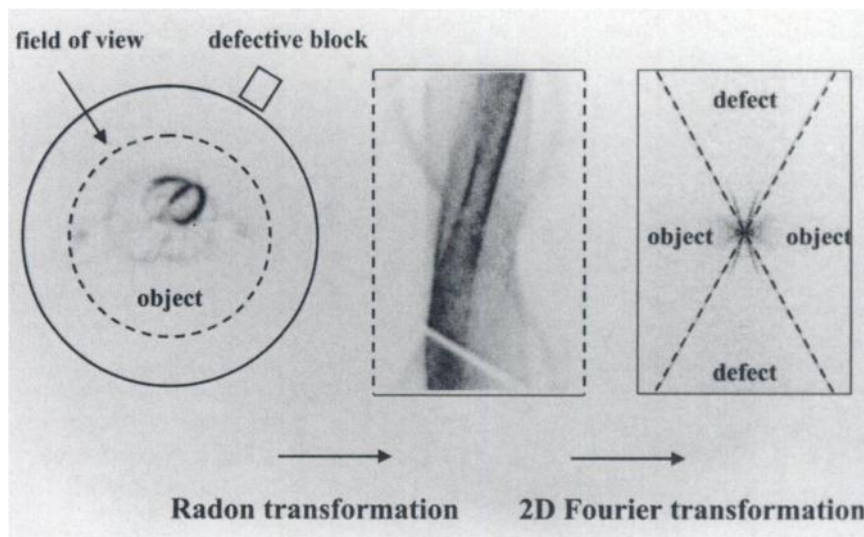


FIGURE 2. Effect of detector defect on filtered backprojection and two-dimensional (2D) Fourier transformation. Fourier transform of consistent sinogram has non-negligible amplitude only inside vertical conic section defined by object radius. Non-negligible entries outside vertical conic section are primarily due to detector defect. If coefficients are set to zero, inverse Fourier transform of remaining coefficients is consistent estimate of noncorrupted projection data.

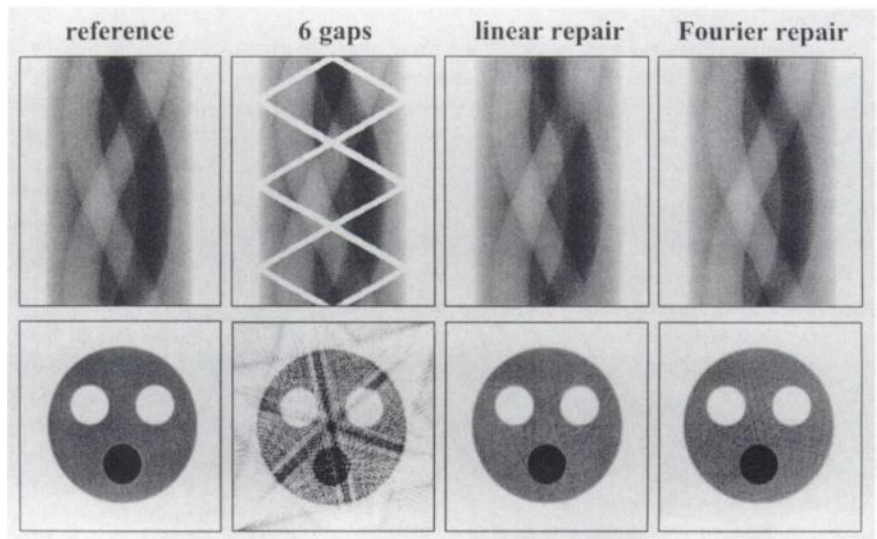


FIGURE 3. Phantom study simulating case of six equidistant detector gaps. Sinograms in top row from left to right: original, corrupted, repaired by linear interpolation and repaired by constrained Fourier space method. Bottom row: corresponding reconstructed images.

methods were applied to the corrupted study. After reconstruction, reference, corrupted and repaired images were compared visually. To quantify the effect of the repair, the root mean square distance of the repaired sinogram p_r from the reference p_0 relative to the root mean square distance of the corrupted sinogram p_c from the reference was computed by:

$$\text{repair}[\%] = 100 \times [1 - d(p_r, p_0)/d(p_c, p_0)]. \quad \text{Eq. 10}$$

Accordingly, the effect of the repair in reconstructed images was quantified. In all cases, normalization, geometric arc correction and attenuation correction were applied before defect simulation and sinogram repair. Reconstruction was performed by filtered backprojection.

RESULTS

The results of phantom and patient studies are presented in Figures 3–6. Each figure shows the original sinogram (reference), the corrupted sinogram, the sinogram repaired by linear interpolation and the sinogram repaired by the

constrained Fourier space method in top rows from left to right. Corresponding images obtained after reconstruction are depicted in bottom rows.

Defect Copy

Results from the investigations using the software phantom simulation of six equidistant defects or gaps existing in all scanners with hexagonal detector arrangement are shown in Figure 3. Six clearly identifiable, symmetrically arranged defects can be observed both in the sinogram and in the reconstructed image. Four neighboring defective blocks, i.e., the loss of an entire detector bucket, would be represented by a broad band on the corresponding sinogram (not shown). The reconstructed image would exhibit severe artifacts.

Consequences from a defective detector bucket in patient studies are presented using myocardial viability studies in a neonate (Fig. 4) and in an adult (Fig. 7), an adult brain study (Fig. 5) and a whole-body tumor acquisition represented by a transverse section in the upper thoracic region (Fig. 6).

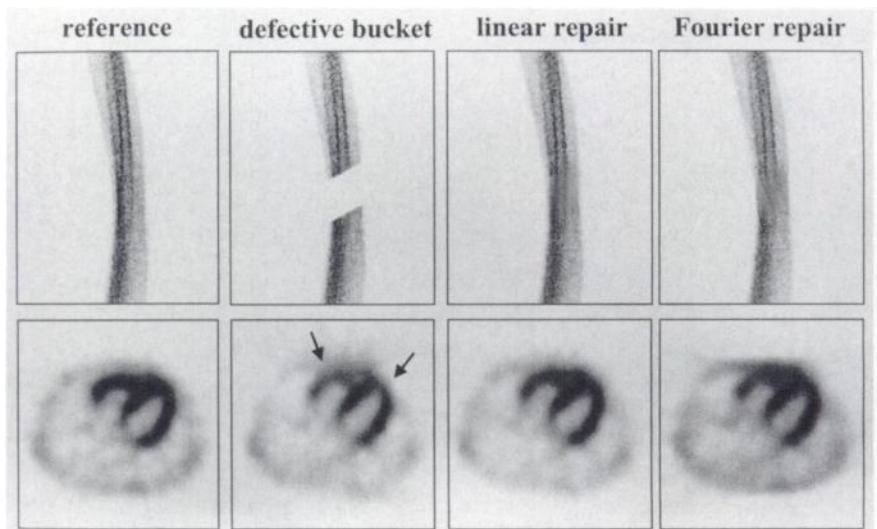


FIGURE 4. Simulation of defective detector bucket in myocardial viability study of 8-wk-old female neonate (weight 4300 g). Sinograms in top row (left to right): original, corrupted, repaired by linear interpolation and repaired by constrained Fourier space method. Bottom row: corresponding reconstructed images. Arrows depict effects of defective detector bucket in reconstructed image.

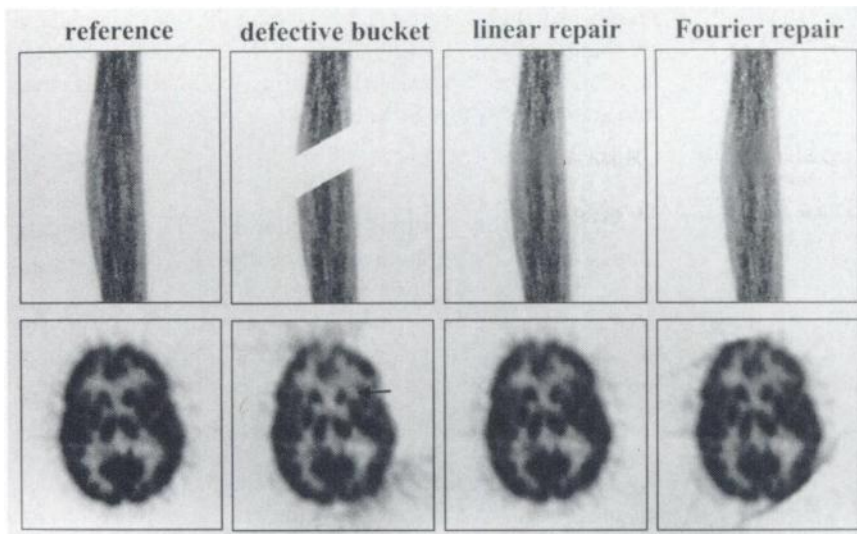


FIGURE 5. Simulation of defective detector bucket in adult brain study. Sinograms in top row (left to right): original, corrupted, repaired by linear interpolation and repaired by constrained Fourier space method. Bottom row: corresponding reconstructed images. Note that side-related differences occurring in basal ganglia (arrows) in corrupted image are almost completely restored by sinogram repair.

Defective sinograms were obtained by manipulating element values in the reference sinogram. In all patient studies, the defective bucket led to significant artifacts (arrows), making the image unreadable (Table 1). Total loss of sensitivity of one or even two blocks did not cause significant artifacts.

Hot Versus Cold Artifacts

The complete loss of sensitivity was compared with a twofold increase in sensitivity of half the crystals of the same detector block and zero sensitivity of the remaining crystals of the block. The comparison was performed by corresponding distortion of the sinogram of the reference oncology study (Fig. 6). The original sinogram (reference), the sinogram representing total loss of sensitivity in one detector block and the sinogram with a twofold sensitivity of half the block are shown in the top row of Figure 8. Corresponding reconstructed images are presented in the

bottom row. The twofold increased sensitivity caused more severe artifacts than did the loss of sensitivity.

Sinogram Repair

Quantitative results of the sinogram repair are given in Figure 7 for both linear interpolation and the constrained Fourier space method.

In the simulations using the software phantom, the effects from the detector gaps were almost completely eliminated by both sinogram repair methods. In the reconstructed images, only minimal local deviations of intensity can be observed (Fig. 3). In the case of a defective bucket, both sinogram repair methods led to clear improvements, but defect elimination was less complete than in the hexagonal model.

In patient studies, sinogram repair applied to the baby heart study (Fig. 4) and the adult brain study (Fig. 5) resulted in images close to the reference. On the other hand,

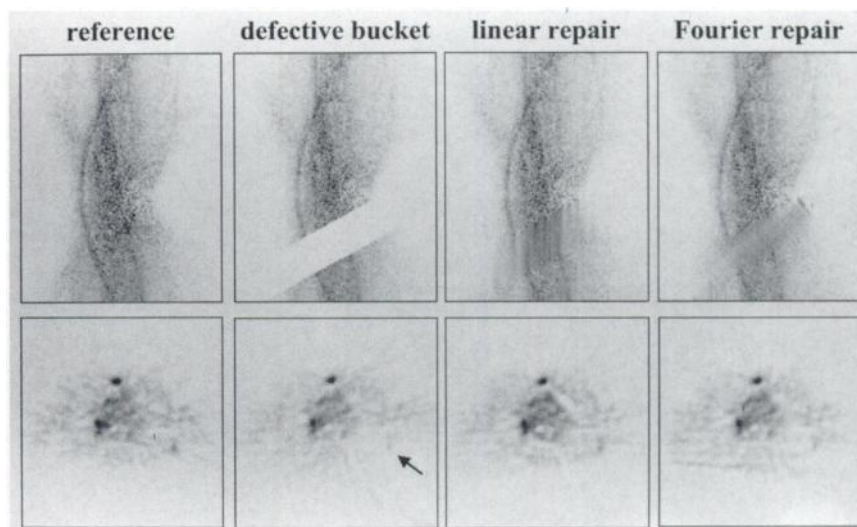


FIGURE 6. Simulation of defective detector bucket in whole-body tumor study represented by transverse slice in upper thoracic region. Sinograms in top row (left to right): original, corrupted, repaired by linear interpolation and repaired by constrained Fourier space method. Bottom row: corresponding reconstructed images. Note effect on detectability of small, low-contrast lesion close to defective bucket (arrow).

TABLE 1
Effect of Sinogram Repair on Choice to Accept or Reject Resulting Image in Detector Defects Simulated in Phantom and Patient Studies

Study	Defect	Physician's choice	
		Without repair	With repair
Phantom	PENN-PET gaps	Reject	Accept
Phantom	Bucket	Reject	Accept
Baby heart	Bucket	Reject	Accept
Adult heart	Bucket	Reject	Reject
Brain	Bucket	Reject	Accept
Tumor	Bucket	Reject	Reject

PENN-PET from UGM Medical Systems, Philadelphia, PA.

correction was not sufficient in the case of the adult heart and in the oncology study (Fig. 6). These results are summarized in Table 1.

Quantitative comparison of the results of both repair methods shows that in all patient studies linear interpolation performed slightly better than did the constrained Fourier space method (Fig. 7). The optimal number of iterations of the constrained Fourier space method ranged from 10 to 30. In the computer phantom simulations, the Fourier approach yielded slightly better results than did linear interpolation after 500 iterations.

Cutting Sinograms Before Constrained Fourier Repair

The effect of cutting sinograms to the object radius and restricting the repair to those lines of response in the defect mask that cross the study object on the results of the constrained Fourier space repair was examined for the brain study presented in Figure 5. Without restricting the repair to the lines of response through the study object, a significant

number of counts were located beyond the object boundary. Without cutting, 95 iterations were required to obtain optimal results, whereas with cutting, optimal results were obtained after as few as 9 iterations.

DISCUSSION

Current quality assurance procedures in PET are sensitive indicators of changes in imaging features. A typical example is the daily determination of the so-called average variance in CTI/Siemens PET scanners. This parameter quantifies the result of the comparison of a reference blank scan acquired during the last setup of the scanner with the daily acquired blank scan. The difference is expressed by the square sum of the differences of the relative crystal efficiencies weighted by the inverse variances of the differences. The sum divided by the total number of crystals is the average variance. If, for an average fan sum of about 20,000 counts, the average variance exceeds 2.5, recalibration of the scanner is recommended. If the average variance exceeds 5.0, calling the manufacturer's service contact is recommended (8,9).

Summarizing the result of the constancy check as one single parameter is supported by the fact that any change of the performance of the scanner results in an increase of the average variance. However, the estimation of the clinical relevance of the particular problem is not supported. Furthermore, the recommended threshold for intervention is rather low for daily practice. Even the defect of one single photomultiplier yields an average variance of only 40 and, therefore, implies cancelation of any further investigations. Under real clinical circumstances, however, unnecessary postponing of patient investigations should be avoided. Delays in the clinical decision process not only result in frustration for the referring physician but also imply additional costs. Strict application of a simple troubleshooting

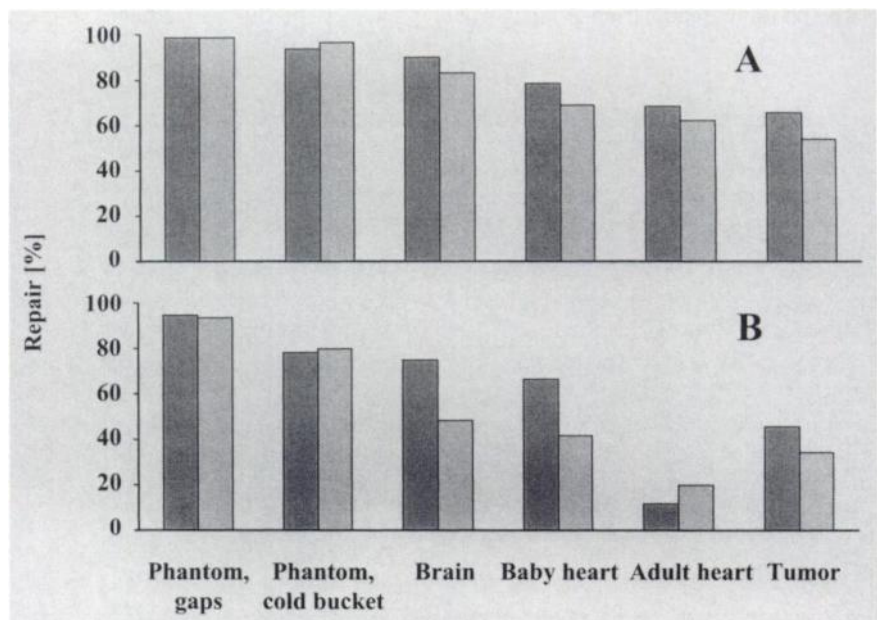


FIGURE 7. Quantitative evaluation of sinogram repair by linear interpolation (dark bars) and Fourier space method (light bars) in sinograms (A) and in reconstructed images (B).

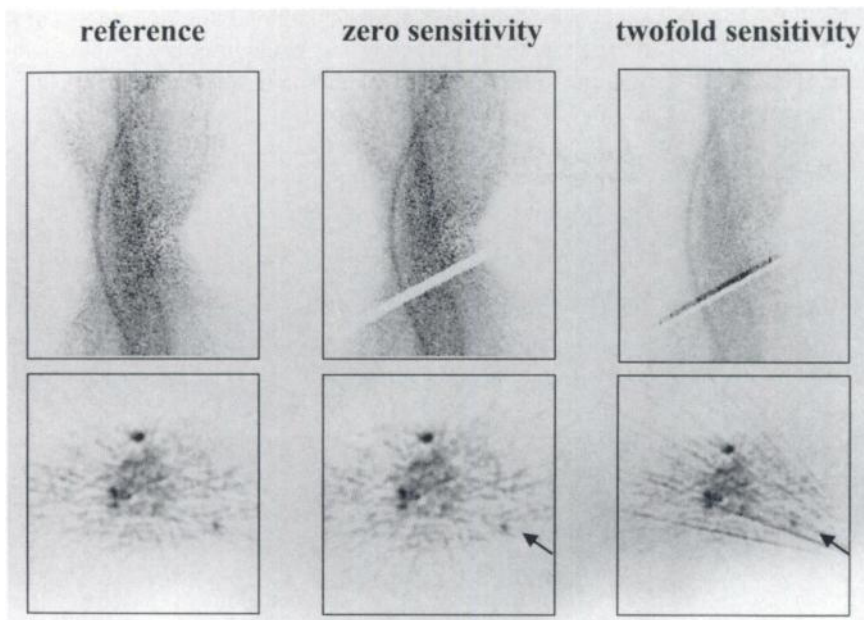


FIGURE 8. Zero sensitivity of single block versus twofold sensitivity of half of crystals of block (zero sensitivity of remaining crystals) in same study as shown in Figure 6. Sinograms in top row (left to right): original, total loss of one block and doubled sensitivity of one block. Bottom row: corresponding reconstructed images. Note effect on detectability of small, low-contrast lesion close to defective block (arrow).

guide that relies on a rather coarse classification according to type (cold or hot) and extent (block or bucket) of the defect (10) is too restrictive in many cases. Therefore, there is a real need for a practical procedure for the correct estimation of the clinical significance of detector problems.

The purpose of the defect copy approach described in this study is the evaluation of the clinical consequences of a detector problem to provide more flexibility in troubleshooting of detector problems. The technique is independent of the specific equipment. The same procedures can be used in principle in any PET scanner. It can also be adapted to SPECT facilities or to CT.

The defect copy method is based on the condition frame. The condition frame can be obtained by dividing any actual scan by a scan acquired with the same source before the appearance of the defect. In daily routine, the blank scan of the daily detector check and the blank scan acquired during the last setup of the scanner are used. Blank scans are acquired using rotating rod or pin sources. Because the orbit of these sources is crossed by all lines of response, the condition frame characterizes the whole field of view of the scanner. In addition, blank scans of the daily detector check and the setup are regularly acquired overnight and, thus, contain a large number of counts, typically about 1000 per sinogram element. This ensures a low level of statistical noise in the condition frame. The actual detector problem can be transferred to a typical patient study by multiplying the sinograms of the patient study acquired before appearance of the defect on an element-by-element basis by the condition frame.

After reconstruction of the corrupted sinograms, images provide a prediction/simulation of image artifacts to be expected in subsequent investigations of the same type. A simple visual comparison of the artificially distorted and the

original images enables the physician to decide whether an image acquisition for this given type of study still serves with acceptable results. Thus, a defect copy helps to decide whether detector repair can be postponed until routine patient investigations are completed.

In this study, a defective detector block or bucket was evaluated in one example each for different types of studies. Certainly, this does not allow general conclusions about the utility of a defective system, although the examples were chosen to represent worst cases. However, the aim of this article is to point out that it might be possible to use a PET system even when the relatively conservative quality control measure indicates a problem and to propose the defect copy method to check if the system works sufficiently for a specific type of study. The aim definitely is not to recommend lowering quality performance standards in PET by making general conclusions about the utility of a system with defective blocks. Nevertheless, based on our observations, the following rules can be stated.

First, an artificially increased sensitivity of detector regions can cause more pronounced artifacts than does a lack of sensitivity of detector blocks. Second, cold detector blocks cause fewer artifacts than expected on the basis of the extent of typical cold diagonal bands in the sinograms. This can be explained by the fact that defective detector regions mathematically act as a sink (or source) of counts far outside the field of view of the scanner (Fig. 2). Therefore, in reconstructed images, artifacts due to defective detectors decrease with increasing ratio of detector-ring radius to field-of-view radius. The diagonal bands in the sinograms are, in fact, parts of a sinoidal pattern. This is because point sources show up as sine curves in the vertical direction in the sinogram. The amplitude of the sinoidal pattern is defined by the radius of the detector ring. Because the sinograms shown

(e.g., Fig. 3) are restricted in the horizontal direction to the transaxial field of view, which has a much smaller radius, only parts of the sinodial pattern can be seen. These parts look very much like straight lines. Third, effects decrease with an increasing distance of the region of interest from the defective detector region. This was shown by effects on different metastases in Figures 6 and 7. A practical consequence of this is that, in the case of defective detectors, nonstandard positioning of the patient, e.g., prone instead of supine, may be helpful. Fourth, a total loss of one or even two blocks of the ECAT EXACT scanner does not cause significant artifacts in reconstructed slices. Therefore, even an average variance of about 100, far exceeding the limit specified by CTI/Siemens, does not necessarily imply that all patient studies for that day must be canceled. Finally, effects of malfunctioning detectors in reconstructed images are expected to depend on the reconstruction algorithm used.

If the defect copy method is applied to a study with measured attenuation correction, the question arises as to how attenuation correction factors are affected by the defect. Attenuation correction implies the quotient of a transmission scan and a blank scan, so that the effects of a defective detector will cancel out. Obviously, this is not true at lines of response with a total loss of sensitivity. However, attenuation correction factors of these zero bins do not matter, because during reconstruction they are multiplied by zeros from the emission scan. Thus, if measured attenuation correction is applied, the original correct attenuation factors can still be used during a defect copy. The effects of count statistics are not considered by this method. Reduced counts in the transmission scan and similarly reduced counts in the blank scan due to a low-sensitivity detector lead to increased noise along the corresponding lines of response.

Theoretically, the most straightforward and, in principle, most accurate method of sinogram repair is to divide sinograms by the condition frame. However, this requires that there be no crystals with zero efficiency (division by zero at the corresponding elements) and that there be no drift of the condition frame in time. Therefore, this method is applicable in special cases only.

In this study, two different approaches of sinogram repair were investigated, i.e., simple linear interpolation and the constrained Fourier space method. Other approaches to sinogram repair and the use of iterative reconstruction algorithms that do not require complete data and, therefore, can be restricted to sinogram data outside the defect mask are discussed elsewhere (11-13).

Both approaches of sinogram repair started with the generation of the defect mask defining which elements of the sinograms were to be repaired. The values of the sinogram elements within the defect mask were then estimated mathematically by the correction method applied. All other elements were assumed to be correct and, thus, remained unchanged. The defect mask was obtained from the condition frame using a limit of variation of $\pm 10\%$. In general, the limit for a sinogram element to be erroneous should be

adapted to the level of statistical noise in the sinograms used to compute the condition frame. If the limit is too tight, data that are within normal variation could be called erroneous. In this study, $9 \times 9 \times 9$ smoothed blank scans with about 1000 counts per sinogram element were used to compute the condition frame. This led to noise in the condition frame of significantly below 5%; thus, the $\pm 10\%$ criterion chosen is appropriate.

Linear interpolation repair is achieved by filling up defective bins by values calculated by linear interpolation of the adjacent correct bins along columns of sinograms (view angle, θ direction), i.e., in a vertical direction. This approach is motivated by the fact that for rotary symmetric objects at the center of the transaxial field of view, all projection views are identical and most detector defects show up as diagonal (close to horizontal) bands in the sinograms. To reduce noise-induced artifacts, sinograms were smoothed before and after interpolation.

The constrained Fourier space method is based on the inherent property of the two-dimensional Fourier transformation of sinograms to almost completely separate counts originating from inside the field of view (the patient) and counts from outside the field of view (the defective detector) in different parts of the Fourier coefficient matrix. Thus, counts originating from defective detectors can be edited, i.e., set to zero, and by an inverse Fourier transformation of the remaining Fourier coefficients, the affected parts of the sinogram can be estimated. Forward and inverse Fourier transformation must be iterated several times, because, in principle, counts originating from the patient or from the defective detector cannot be separated completely.

In phantom studies, both methods of sinogram repair performed equally well. However, sinogram repair did much better in the PENN-PET situation with six equidistant detector gaps (Fig. 3) than in the case of four neighboring defective detector blocks, although the number of affected lines of response was identical in both cases.

In real patient studies, the quality of repair for detector defects affecting up to 15% of a sinogram, i.e., one defective detector bucket, depended significantly on the size of the study object (Fig. 7). For small study objects, such as the baby heart (Fig. 4) or the adult brain (Fig. 5), with the object at the center of the transaxial field of view, results were satisfactory. In contrast, in large study objects, such as an adult heart (with background in the thorax) or the whole-body acquisition, results, in general, were not satisfactory (Fig. 6). This agrees with the results of Fujieda et al. (7), because error correction worked particularly well for the phantom considered in their work. Linear interpolation with smoothing performed slightly better than our implementation of the constrained Fourier space method in the patient studies presented here. As the simulations with the computer phantom suggest, this was because the optimal number of iterations was rather small in cases of inconsistent and noisy projection data. Amplification of errors and generation of artifacts prevented further convergence of the Fourier inter-

polation. However, generation of artifacts can be reduced by some refinement of the method. The result of sinogram repair in reconstructed images measured by the repair in percent as defined in this article does not depend only on the reconstruction algorithm but also on reconstruction zoom and x- and y-offset. This explains the difference between the repair in the reconstructed images of an adult heart and the tumor study (Fig. 7). The heart study was reconstructed with a zoom factor of 2.0 and an offset of about 4 cm toward the defective bucket. The tumor study was reconstructed with a zoom factor of 1.0 and with no offset.

Several observations concerning the constrained Fourier space method can be made. First, cutting sinograms to the object radius significantly improved results. In addition, convergence of the constrained Fourier space method was accelerated, and computation time for each iteration was reduced. Computation time saved was dependent on the object radius, the transaxial field of view of the scanner, the number of projection bins per view and the Fourier transform algorithm. For example, in an adult brain scanned with the ECAT EXACT, the number of projection elements per view could be reduced from 160 to 60. By applying Fast Fourier transformation, computation time per iteration was then reduced to 30% ($=60/160 \times \ln_2 60/\ln_2 160$). Second, using the constrained Fourier space method, sinogram elements affected by the defect should be set to zero before starting the iteration, particularly in cases of hot artifacts. This limits the number of bad counts to be eliminated. Third, concerning the convergence of the constrained Fourier space method, good repair results were obtained after as few as 3 iterations. Further iterations yielded minor improvements only. When applied to real patient data, results began to worsen after 10–30 iterations. Therefore, in practice, the number of iterations should be restricted to 3. Fourth, repair results depended on the size of the sinogram region in which the repair acted: the smaller the better. Therefore, in addition to cutting sinograms to the object radius, the repair should be restricted to the lines of response in the defect mask that cross the patient. Last, because the constrained Fourier space method makes use of a specific property of sinograms, data must be consistent throughout but for inconsistencies caused by the defect. Therefore, normalization, geometric arc correction and attenuation correction are mandatory before the repair. The most obvious property of sinograms that does not hold for attenuated data is that the sum of the projection elements is the same for all views. Other less evident

properties of sinograms are discussed in detail elsewhere (14). Therefore, as expected, the constrained Fourier space method was not applicable to strongly inconsistent data, i.e., in non-attenuation-corrected data of the adult thorax, the iteration did not converge at all. Results became worse, starting from the second iteration.

CONCLUSION

The described method of simulation of given detector defects in sinograms of real patient studies is an easy-to-perform tool for the evaluation of clinical consequences of a detector defect and is completely independent of the individual technical setting. It accurately visualizes the effect of a current defect with respect to the individual situation of study type, acquisition mode and reconstruction parameters. This allows one to decide whether an individual patient study can be performed or must be postponed. Even with significant detector defects, sinogram repair may make possible image acquisition with only limited loss of quality.

REFERENCES

1. Wienhard K, Eriksson L, Grootoink S, Casey ME, Pietrzyk U, Heiss WD. Performance evaluation of the positron scanner ECAT EXACT. *J Comput Assist Tomogr.* 1992;16:804–813.
2. Klingensmith WC III, Eshima D, Goddard J. *Nuclear Medicine Procedure Manual 1997–98.* Englewood, NJ: Wick Publishing; 1997.
3. Karp JS, Muehlechner G, Mankoff DA, et al. Continuous-slice PENN-PET: a positron tomograph with volume imaging capability. *J Nucl Med.* 1990;31:617–627.
4. *ECAT software 6.5B* [computer program]. Process-blank, version 2.4. Knoxville, TN: CTI PET Systems; 1992.
5. Edholm PR, Lewitt RM, Lindholm B. Novel properties of the Fourier decomposition of the sinogram. *Proc Soc Photo-Opt Instrum Eng.* 1986;671:8–18.
6. Karp JS, Muehlechner G, Lewitt RM. Constrained Fourier space method for compensation of missing data in emission computed tomography. *IEEE Trans Med Imaging.* 1988;7:21–25.
7. Fujieda I, Heiskanen K, Perez-Mendez V. Versatility of the CFR algorithm for limited angle reconstruction. *IEEE Trans Nucl Sci.* 1990;37:585–588.
8. Spinks T, Jones T, Heather J, Gilardi M. Quality control procedures in positron tomography. *Eur J Nucl Med.* 1989;15:736–740.
9. *ECAT software 6.5B* [computer program]. Sysqual, version 2.10. Knoxville, TN: CTI PET Systems; 1992.
10. Currie G, Baily D. To scan or not to scan? *The ECAT Post.* 1993;3:2.
11. Ollinger JM, Karp JS. An evaluation of three algorithms for reconstructing images from data with missing projections. *IEEE Trans Nucl Sci.* 1988;35:629–634.
12. Huang S-C, Yu D-C. Capability evaluation of a sinogram error detection and correction method in computed tomography. *IEEE Trans Nucl Sci.* 1992;39:1106–1110.
13. Enghardt W, Fromm WD, Manfrass P, Schardt D. Limited-angle 3D reconstruction of PET images for dose localization in light ion tumor therapy. *Phys Med Biol.* 1992;37:791–798.
14. Natterer F. *The Mathematics of Computerized Tomography.* Stuttgart, Germany: John Wiley & Sons; 1986:9–18.